Electron cloud effects on an intense ion beam in a four solenoid lattice

J.E. Coleman
Department of Nuclear Engineering, University of California at Berkeley, 4155 Etcheverry Hall, MC 1730, Berkeley, CA 94720, USA.

P.A. Seidl, E. Henestroza, P.K. Roy, and J.L. Vay
Lawrence Berkeley National Laboratory, 1 Cyclotron Road, Berkeley, CA-94720, USA.

I. Haber
University of Maryland, College Park, MD 20742-3511, USA.

A.W. Molvik and W.M. Sharp
Lawrence Liveremore National Laboratory, Livermore, California 94550, USA.

D.R. Welch
Voss Scientific, Albuquerque, NM 87108, USA.
(Dated: July 16, 2007)

The Solenoid Transport Experiment (STX) at LBNL successfully demonstrated the transport of a space-charge dominated ion beam in a two-solenoid lattice. Initial experiments showed a strong dependence of electron cloud effects on solenoid field strength. A current-reducing aperture, two solenoids and in-bore diagnostics were added to the two-solenoid lattice in order to study electron cloud effects more closely. Experiments were conducted with a 10 μs, singly charged potassium ion bunch at an ion energy of 0.3 MeV and currents of 26 mA and 45 mA. A qualitative comparison of experimental and calculated results are presented, including a comparison of the effects of manipulating electrons on the beam dynamics, quantifying beam-induced gas desorption, ionization, and electron effects.

PACS numbers: 52.59.Sa, 41.75.Ak, 41.85.Lc, 41.85.Ja, 29.27.Bd, 29.30.Aj, 34.50.Dy, 79.20.Rf

I. INTRODUCTION

Space-charge dominated ion beams used in the low energy end of an accelerator to drive fusion targets face a number of unique challenges. One of particular interest to the general accelerator community is beam degradation due to electron cloud and gas effects [1–10].

Mismatched portions of a beam, such as beam halo, photons hitting the beam pipe, and anything that obstructs the path of the beam, desorbs gas and electrons [11–14]. The desorbed gas expands into the beam path close to the sound speed and subsequently becomes ionized [15]. In some cases the electron and ionized neutral densities can approach the beam density and significant changes in the charge collected on diagnostics, emittance growth, and fluctuations in the beam envelope are seen [16, 17].

For solenoid transport of space-charge dominated ion beams the predominantly axial fields in the center of the magnets and the radial fields in between magnets provide an easier means for electrons to be pulled in by the beam potential and stay there. These fields also present difficulties in suppressing electrons when intercepting the beam with diagnostics.

The ion species used for the STX on the Neutralized Drift Compression Experimental beamline (NDCX) was a singly charged, 300-kV, 26-45 mA potassium ion beam [17–19]. A solenoid field close to 3 T was necessary in the first magnet to match or overcome the beam space charge force. The exact tune used in the lattice was chosen based on the desired envelope and to avoid scraping. This included compensating for beam halo and centroid motion.

II. FOUR-SOLENOID EXPERIMENT

Two more solenoids were added to the two-solenoid lattice on the NDCX beamline (Fig. 1). The two additional solenoids were also 50-cm long, had an identical construction to those used in the two-solenoid experiment, and the spacing in between all of the magnets was about 9 cm [17, 20]. The observation that intercepting the beam in a strong magnetic field aided electron cloud and gas effects in degrading the beam quality in the two-solenoid experiment was accounted for in this four-solenoid lattice. So the same 29-cm drift distance was used between the exit of the four-solenoid lattice and the intercepting diagnostics.

Initial tests with the four-solenoid lattice were done with a current-reducing aperture that reduced the 45-mA beam to 26 mA. The focusing lattice in Figure 2(a) was chosen to give the desired envelope for the 26-mA beam in Figure 2(b). All of the same diagnostics used in the two-solenoid experiment were used here [17]. Despite having the additional drift distance from the trans-

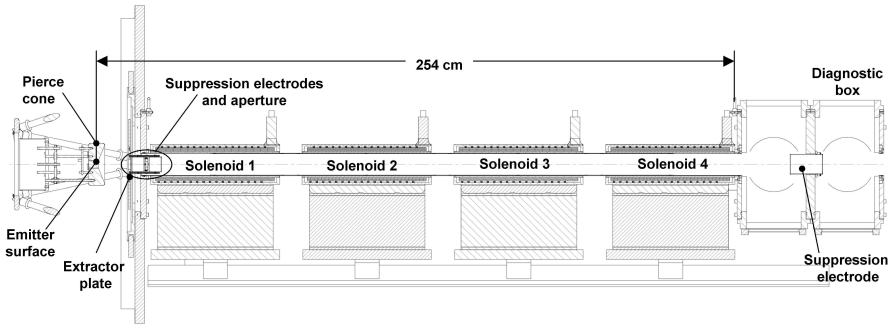

FIG. 1: Elevation view of the Four-Solenoid Experiment.

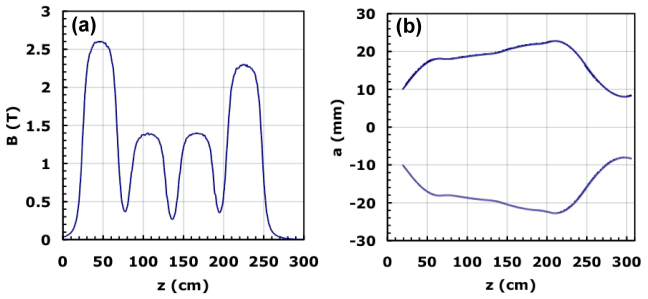

FIG. 2: (a) Focusing lattice used to obtain the: (b) ideal envelope for the 26-mA beam.

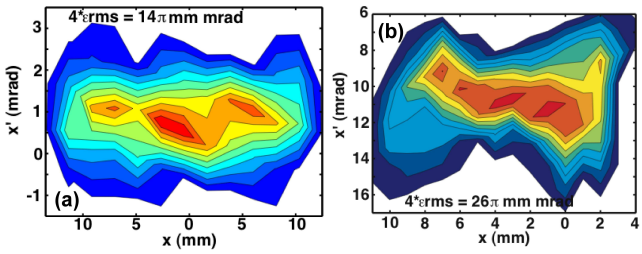

FIG. 3: Sheared phase space distribution integrated over a 500 ns gate in the middle of the 10 μs beam pulse: (a) 15 cm downstream of the exit of the extractor (no solenoids); (b) 39 cm downstream of the exit of four solenoids.

port lattice to the diagnostic plane the beam quality was not as expected. The emittance for the apertured beam was 80% larger than what was measured directly downstream of the gun without any focusing (Fig. 3). The beam envelope also had slight time dependence but the envelope remained converging and the variation in radius was less than 2 mm (Fig. 4). These observations indicated the aperture itself may have been contributing to electron cloud and gas effects, experiments with electron cloud diagnostics will allude to this.

III. ELECTRON CLOUD DIAGNOSTICS

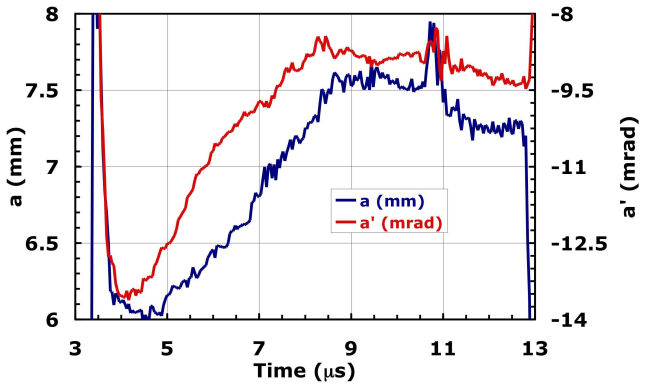

FIG. 4: Beam envelope 39 cm downstream of the exit of four solenoids as a function of time.

Extensive studies of electron cloud and gas effects in the four-solenoid lattice were done with the apertured 26-mA beam using new in-bore diagnostics. These electron cloud diagnostics consisted of 4 short (8.45-cm long) cylindrical electrodes in the center of each solenoid magnet (solenoid electrodes) and the 3 longer (25.4-cm long) cylindrical electrodes in the gaps between magnets (gap electrodes). The gap electrodes were strategically placed to intercept the maximum amount of expanding magnetic flux (Fig. 5). The 13-cm long cylindrical electrode that was just upstream of the intercepting diagnostics was moved 29 cm upstream into the exit of solenoid 4. A pair of parallel plates was used in place of this cylindrical electrode just upstream of the intercepting diagnostics to suppress electrons.

The diagnostics measured a positive capacitive image charge of the beam as it entered the diagnostic and negative capacitive image charge of the beam as it exited (Fig. 6). These capacitive signals are proportional to the derivative of the beam current. The signals are displaced in time due to the time of flight of the beam to each electrode. The width of the spikes alternated between narrow and wider, corresponding to the short solenoid electrodes and the longer gap electrodes. Measurements showed a growth in the positive capacitive signal as the beam propagated axially due to overtaking in the beam

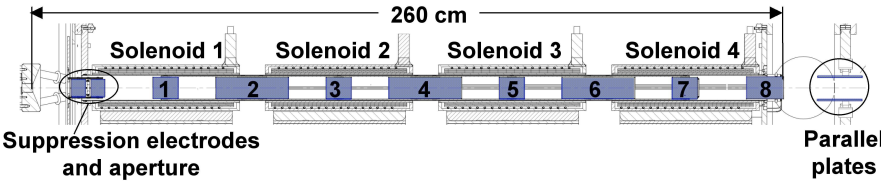

FIG. 5: Layout of the electron trap (Trap 1), electron cloud diagnostics (1 - 8), and parallel plate diagnostic relative to the four-solenoid lattice. All the diagnostics have cylindrical symmetry except for the parallel plate diagnostic.

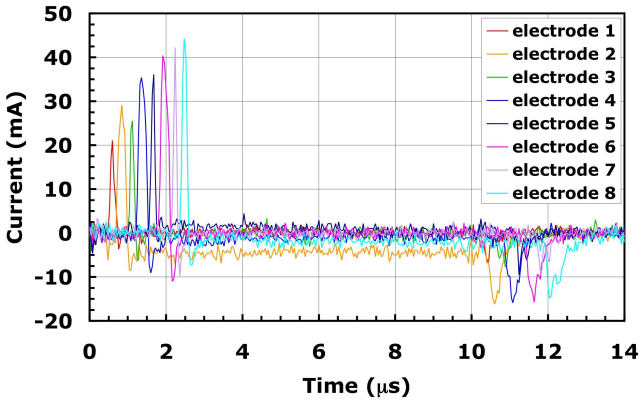

FIG. 6: Electron cloud diagnostic signals as a function of time.

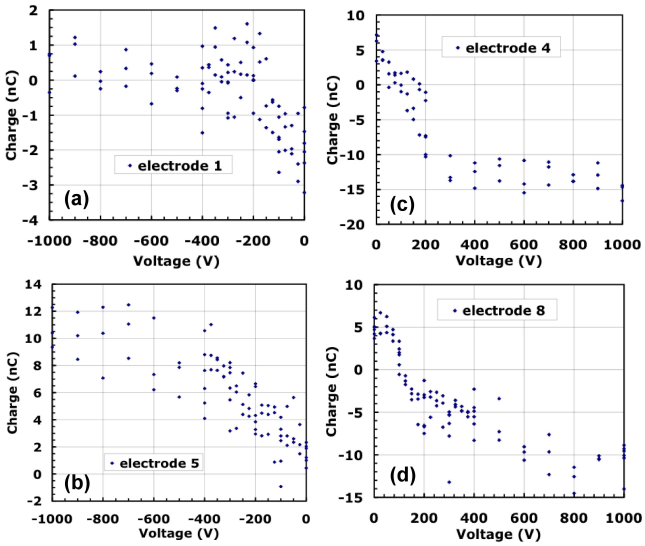

FIG. 7: Charge collected as a function of bias voltage for: (a) electrode 1; (b) electrode 5; (c) electrode 4; (d) electrode 8.

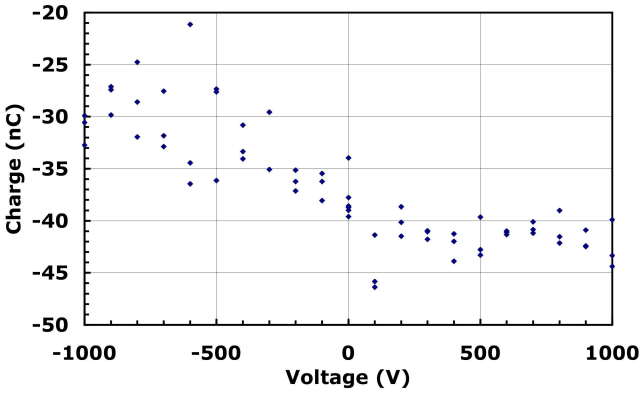

FIG. 8: Charge collected as a function of bias voltage for electrode 2.

head. The electrodes collected charge throughout the pulse depending on the bias configuration and location of the diagnostic along the focusing lattice.

These electrodes were independently biased between ±1 kV. The solenoid electrodes were biased negatively to repel electrons, while the gap electrodes were biased positively to clear electrons from intercepted field lines and suppress emission. Reversing the biases trapped electrons that were emitted from the gap electrodes between magnets. Results of operating the diagnostics to clear electrons from the lattice showed charge collection began to saturate for voltage biases $|V| \geq 600$ V (Fig. 7).

Some of the evidence that the aperture was contributing to electron cloud and gas effects was seen from the charge collected on the most upstream gap electrode 2 (Fig. 8). Electrons were collected on this electrode regardless of the bias voltage and the threshold was reached just above +100. This electrode was magnetically connected to the aperture, because most of the field-lines from the first solenoid that intersected this electrode also intersected the aperture. Any electrons made by the beam at the aperture would have most likely been tied to these fieldlines and be collected on electrode 2.

The impact of clearing electrons on the beam quality was evident from measurements of the transverse beam distribution and phase space (Fig. 9). The transverse beam distribution of the suppression case had a smaller circular distribution compared to the larger and more irregular shapes of the other two cases. Collecting electrons in the gaps between solenoids (clearing) decreased the unnormalized emittance over 25% versus grounding the electrodes and trapping electrons inside the solenoids increased the unnormalized emittance more than a factor of five.

Further evidence of efficient clearing of electrons was shown in time dependent phase space measurements of the beam (Fig. 10). The transverse phase space of the

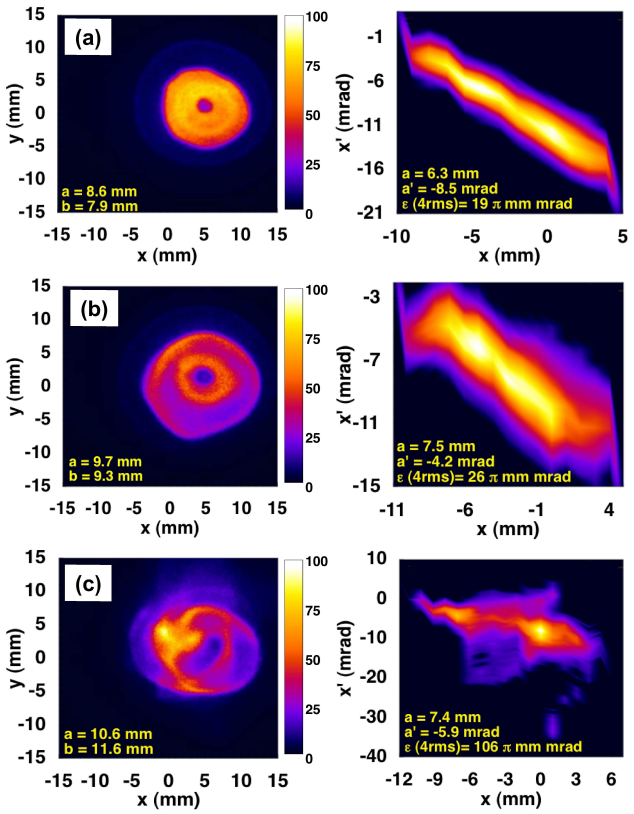

FIG. 9: Left column: measured transverse beam distribution; right column: measured transverse phase space (note scale differences) for: (a) clearing case; (b) grounded case; (c) trapping case.

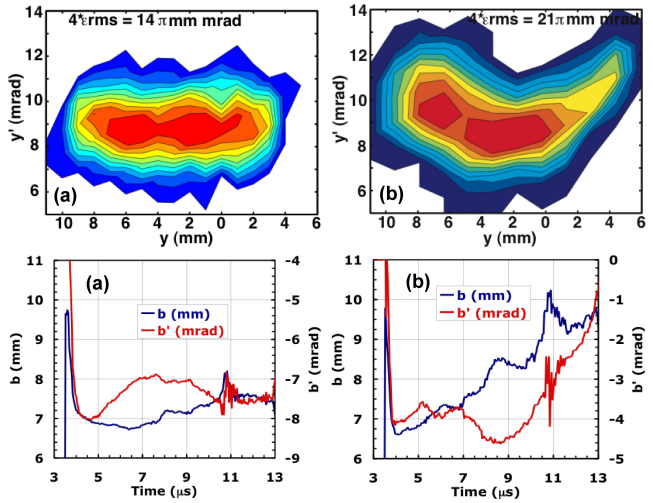

FIG. 10: Top row: measured sheared phase space distribution; bottom row: measured envelope as a function of time for: (a) clearing case; (b) grounded case.

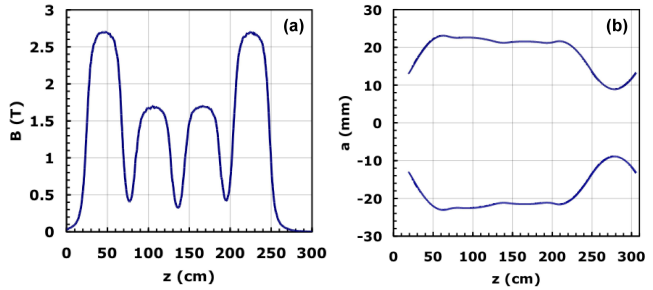

FIG. 11: (a) Focusing lattice used to obtain the: (b) ideal envelope of 43-mA beam.

clearing case had a uniform distribution compared to the larger and more irregular shape of the case where the electrodes were grounded. Collecting electrons in the gaps between solenoids (clearing) matched the emittance of the beam extracted from the diode (14 π mm mrad) and was 30% less than the grounded electrode case. Clearing electrons also removed the time dependence in the beam envelope and parameters agreed well with values calculated by solving the envelope equation. The time dependence observed in the beam envelope without electron cloud suppression was likely due to partial neutralization of the beam space charge. If the electron density was high enough at any location in the lattice that portion of the beam envelope would have focused more easily as was seen in the two-solenoid experiment [17]. The variation in the beam envelope of the clearing case on the left was within the resolution of the measurement, which is less than a millimeter and exactly 1 milliradian. Additional random error that can be factored into these measurements is electrical noise that can be larger than the normal signal to noise ratio of 30.

The evidence that the aperture was a leading source of electrons and gas was complemented with measurements without the aperture. A separate focusing lattice [Fig. 11(a)] was used in order to compensate for the higher beam current and in order to yield an envelope that did not scrape [Fig 11(b)].

The measurements with the unapertured 45-mA beam show there was an insignificant difference between the cases when the diagnostics were grounded versus when they were biased to clear electrons; and negligible charge is collected on the electron cloud diagnostics for the 45-mA beam when compared with the clearing case for apertured 26-mA beam (Table 1 and Fig. 12). The highlighted cases in Table 1 show the most significant differences in the charge collected on individual electrodes. Those electrodes with 2 nC or less of collected charge were well within the electrical noise (error bars) of the diagnostics. This indicated that clearing electrons might not be necessary if there is no other source of electrons and gas besides the aperture.

Examining the charge collected on the electrodes due to capacitive effects for the 45-mA beam demonstrated the difference in electrode length. The shorter electrodes had 4 nC of induced charge, while the longer electrodes showed about 10 nC. The accumulated charge (difference between end and beginning of beam pulse) for the

TABLE I: Comparison of the charge collected on the electron cloud diagnostics for the 45-mA beam and apertured 26-mA beam for the clearing case.

	26-mA beam	45-mA beam
Diagnostic	**Charge (nC)**	**Charge (nC)**
electrode 1	1.39	-0.51
electrode 2	-41.08	-1.06
electrode 3	-1.70	0.35
electrode 4	-11.24	-0.94
electrode 5	9.00	-0.06
electrode 6	-1.50	-2.22
electrode 7	-1.37	-0.85
electrode 8	-18.69	-0.35
Total Charge (nC)	85.97	6.33

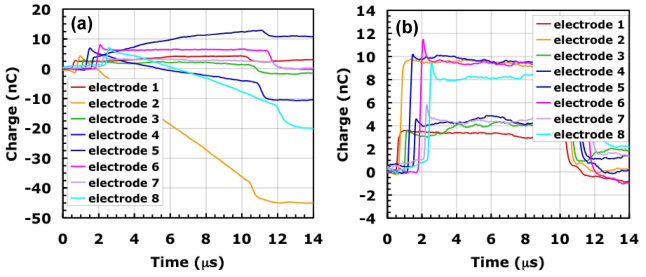

FIG. 12: Comparison of the charge collected on the electron cloud diagnostics for the: (a) 45-mA beam and; (b) apertured 26-mA beam for the clearing case.

unapertured case showed a >10x reduction compared to the apertured beam, in spite of almost twice the beam current and a larger beam envelope.

The measurements without the aperture in this four-solenoid lattice showed a 50% increase in emittance from that measured at the gun and after two solenoids (Fig. 13). As stated above electron cloud effects appear to be small for this unapertured beam case and time dependence in the beam envelope is also small. The distortions in the phase space distribution help add to the emittance and are most likely due to the unstable centroid motion of the beam throughout the focusing lattice. This points out the importance of controlling the centroid motion in a focusing lattice and the implication that a longer transport system with more focusing elements would be more strongly impacted.

IV. CENTROID MOTION

An examination of Figures 9, 10, and 13 proved that the beam envelope was offset by several millimeters and milliradians. Centroid offsets were also observed in the two-solenoid experiment and it appeared they might have grown due to the increase in misaligned focusing elements [17, 21, 22]. Individually reversing the field on

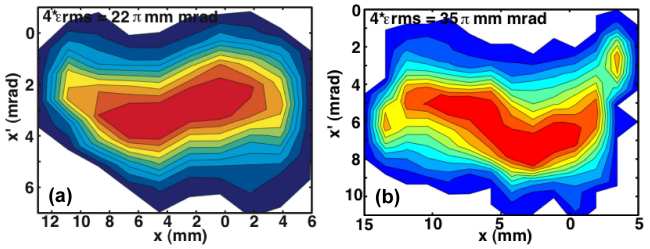

FIG. 13: Sheared phase space distribution of the unapertured beam integrated over a 500 ns gate in the middle of the 10 μs beam pulse: (a) 39 cm downstream of the exit of two solenoids; (b) 39 cm downstream of the exit of four solenoids.

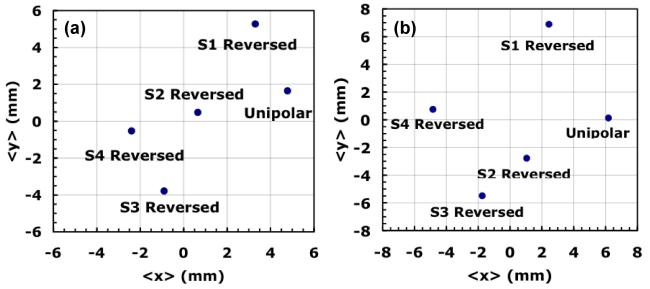

FIG. 14: First moments of the transverse beam distribution integrated over a 500 ns gate in the middle of the 10 μs beam pulse 55 cm downstream of the exit of four solenoids for the: (a) apertured 26-mA beam; (b) 45-mA beam.

each solenoid from having a unipolar lattice helped quantify the centroid dependence on each magnet. This was done for both the apertured 26-mA beam and the 43-mA beam; slightly different results were seen for each situation (Fig. 14). The information from one magnet could not be decoupled from the others because each of the iterations depended on the kicks given by each magnet but it was still instructive to see the impact that each magnet had on the beam.

V. QUANTIFYING ELECTRON EMISSION, GAS DESORPTION AND IONIZATION

A pair of polished stainless steel parallel plates 15 x 15 cm^2 spaced about 7.5 cm apart (Fig. 15) were used to make measurements of desorption, ionization, and secondary emission coefficients with the apertured 26-mA beam. Two configurations were used with the plates: first both plates were biased negatively to suppress electrons and second the plates were biased as a positive dipole to sweep electrons and ionized gas. The plates were strategically placed upstream of all the intercepting diagnostics and biased from 0 to 10 kV in 1 kV intervals.

Two separate diagnostics, a polished stainless steel plate and a polished copper plate intercepted the beam. Each of the plates was at least 4-cm wide to fully ac-

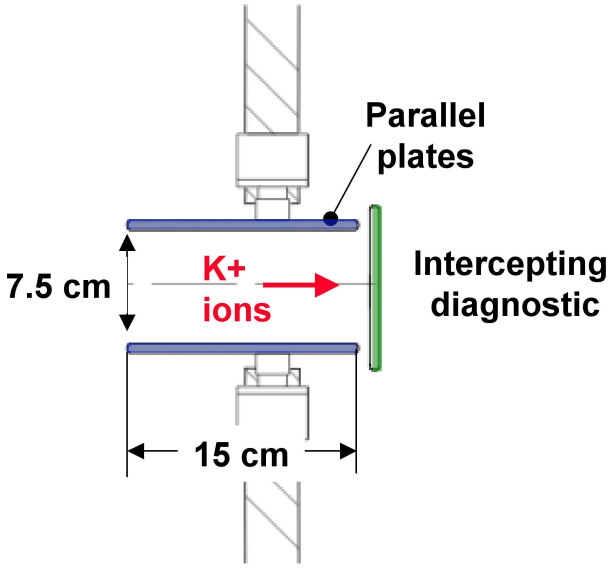

FIG. 15: Sketch of the experimental setup using the parallel plates to measure desorption, ionization, and secondary emission coefficients.

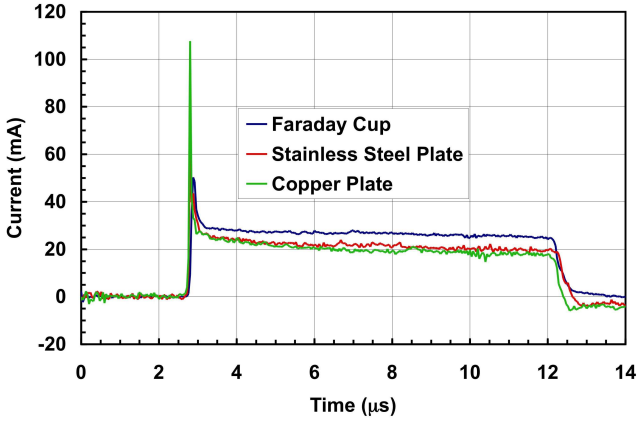

FIG. 16: Beam current signals collected by the Faraday cup (blue), polished stainless steel plate (red), polished copper plate (green).

commodate the 15-cm beam (Fig. 10) and could be capacitively monitored. The purpose of using the two separate materials was to test whether the amount of gas desorbed and electrons emitted was material dependent. The signal provided by the intercepting diagnostic was similar, but not exactly the measured beam current due to non-beam ion and electron species in the vicinity of the diagnostic (Fig. 16).

With both parallel plates biased negatively most of the gas desorbed from the intercepting plate and subsequently ionized was directly measured. H_2 gas was the likely candidate of gas to be desorbed from stainless steel by beam ions [14]. The calculated time for a positive current to appear on the suppressor due to ionized H_2 was about 1 μs. On the STX there was a positive capacitive

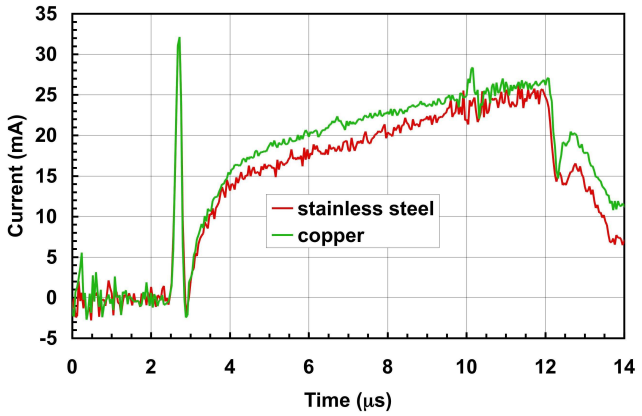

FIG. 17: Ion current signals collected on the parallel plates when intercepting the beam with a polished stainless steel plate (red); and a polished copper plate (green).

image charge when the beam passed through the diagnostic at 2.5 μs followed by a rising positive current less than 1 μs later (Fig. 17). This was seen when intercepting the beam with both a stainless steel plate and a copper plate. The gas initially desorbed and ionized, measured between 3 and 4 μs, was less than 30% of the K^+ ion current with the plates grounded and increased linearly to 70% when the plates were biased negatively to 10 kV.

The slope of the ion current after 4 μs is proportional to the product of the desorbed gas density (n_H) and the ionization cross section (σ_{iz}). This slope increased logarithmically with the voltage used on the plates and using the measured σ_{iz} of 1.6 x 10^{-20} m^2 [13] for the -5 kV case shown in Figure 17 a gas density, $n_H \sim 10^7$ cm^{-3}, slightly less than the beam density ($n_{K+} \sim 10^8$ cm^{-3}) was extracted. The total ion current from the gas desorbed off of the stainless steel and the copper plates only differed by a few percent and was close to 90% of the total K^+ ion current.

Biasing the plates in a positive dipole configuration collected secondary electrons on the positive plate and a fraction of the desorbed and further ionized hydrogen on the grounded plate. This experiment provided the number of electrons released per ion for normal incidence (γ_{se}). The subsequent number of electrons due to ionization can be inferred from the measurement. A positive capacitive image charge appeared when the beam passed through the diagnostic at 2.5 μs followed by an almost instantaneous negative capacitive spike from secondary electrons released from the intercepting plate by the beam head (Fig. 18). Once the head of the beam had passed the beam current and envelope stabilized enabling an accurate determination of the number of secondary electrons. The secondary emission coefficient (γ_{se}) increased logarithmically from about 5 when the plate was at +1 kV to about 9 when the plate was biased to +10 kV. γ_{se} for cases shown here were 8.5 for normal incidence on stainless steel and 7.7 on copper with a bias of

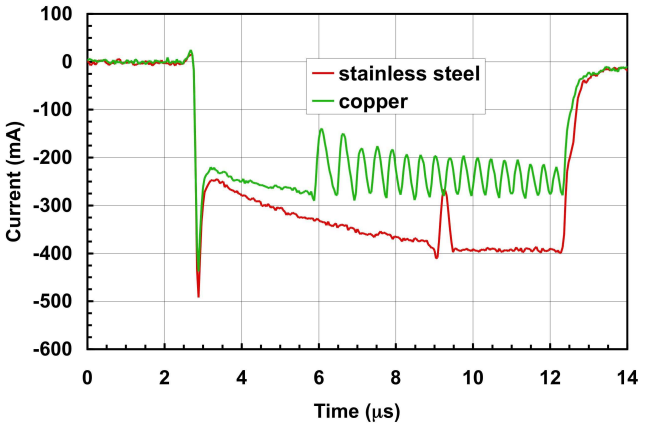

FIG. 18: Electron current signals collected on the positively biased plate when the beam is intercepted with a polished stainless steel plate (red); and a polished copper plate (green).

+5 kV on the dipole plate.

The accumulated electron current thereafter had a slope in time that was proportional to the product of the electron density (n_e) and the ionization cross section (σ_{iz}). This slope also increased logarithmically with the dipole voltage and using the ionization cross section stated above yielded an electron density close to the beam density ($n_e \sim 10^8$ cm^{-3}).

The total electron current accumulated when intercepting the beam with the copper plate was 30% less than when it was intercepted with stainless steel regardless of voltage. When the stainless steel plate intercepted the beam a small positive spike was observed at 9 μs, which was believed to be a sheath of $H_2{}^+$ that was forced to the positive plate. Intercepting the beam with the copper plate displayed different phenomena; a sheath oscillation was observed at 6 μs. This demonstrated that there was a clear dependence of the charge collected by the diagnostics and the material the beam was normally incident upon.

VI. CONCLUSIONS

We were able to successfully control electrons in these four-solenoid experiments despite the aperture being a clear source of electrons and gas. Beam centroid motion continues to be a problem and may be the cause of the emittance growth with the unapertured beam. We plan to use crossed dipoles in each of the three gaps between the solenoids, for a total of 3-x and 3-y dipoles to correct the beam centroid motion.

The beam also has a hollow center and a substantial halo as seen in the two-solenoid experiments. Examining the ion source geometry for any misalignments and the uniformity of the magnetic field at the emitter surface are crucial to improving the beam quality. Making the diode a field free region may remove these discrepancies in the beam quality itself.

We have begun to quantify the amount of electrons and gas born when the beam is normally incident upon a surface. We have also shown the dynamics of the gas desorption, ionization, and secondary emission is dependent on the incident material.

All of this information needs to be well understood if solenoids are going to be used in the low energy end of an accelerator to drive fusion targets.

Acknowledgments

This work was supported by the Director, Office of Science, Office of Fusion Energy Sciences, of the U.S. Department of Energy under Contract No. DE-AC02-05H11231. We wish to thank Tak Katayanagi, Eugene Flor, Michael Dickinson, Cory Lee, Wayne Greenway, Matthaeus Leitner, Will Waldron, David Baca, Craig Rogers, Ed Romero, and Andy Faltens for their continued technical support.

[1] G. Budker, G. Dimov, and V. Dudnikov, Sov. At. Energy **22**, 5 (1967).
[2] O. Gröbner, in Proceedings of the 10th International Conference on High-Energy Accelerators, Protvino, Russia (Institute of High Energy Physics, Protvino, 1977), p. 277.
[3] M. Izawa, Y. Sato, and T. Toyomasu, Phys. Rev. Lett. **74**, 5044 (1995).
[4] K. Ohmi, Phys. Rev. Lett. **75**, 1526 (1995).
[5] W. T. Weng et al., in Proceedings of the Particle Accelerator Conference, Vancouver, Canada, 1997, p. 970, http://www.JACoW.org/.
[6] R. J. Macek et al., in Proceedings of the Particle Accelerator Conference, Chicago, Illinois, 2001, p. 688, http://www.JACoW.org/.
[7] M. A. Furman, LBNL Report No. 50765, 2002.
[8] S.Y. Zhang et al., in Proceedings of the European Particle Accelerator Conference, Lucerne, Switzerland, 2004, p. 947, http://www.JACoW.org/.
[9] J.W. Flanagan et al., Phys. Rev. Lett. **94**, 054801 (2005).
[10] R.J. Macek and A. A. Browman, in Proceedings of the Particle Accelerator Conference, Knoxville, Tennessee, 2005, p. 2547, http://www.JACoW.org/.
[11] A.W. Molvik et al., Phys. Rev. ST Accel. Beams **7** 093202 (2004).
[12] M. Kireeff Covo et al., Phys. Rev. ST Accel. Beams **9** 063201 (2006).
[13] M. Kireeff Covo et al., Phys. Rev. Lett. **97** 054801 (2006).
[14] A. W. Molvik et al., Phys. Rev. Lett. **98** 064801 (2007).
[15] F.M. Bieniosek (to be published).
[16] W.M. Sharp et al., Nucl. Instrum. Methods Phys. Res. A **577**, 146 (2007).

[17] J.E. Coleman et al.,
[18] P.K Roy et al., Phys. Rev. Lett. 95 234801 (2005).
[19] P.A.Seidl et. al., Nucl. Instrum. Methods Phys. Res. A **577**, 215 (2007).
[20] D. Shuman et al., in Proceedings of the Particle Accelerator Conference, Knoxville, Tennessee, 2005, p. 3798, http://www.JACoW.org/.
[21] Y.-J. Chen et. al., Nucl. Instrum. Methods Phys. Res. A **292**, 455 (1990).
[22] Y.-J. Chen, Nucl. Instrum. Methods Phys. Res. A **398**, 139 (1997).
[23] Y.-J. Chen et. al., in Proceedings of the Particle Accelerator Conference, San Francisco, CA, 1991, p. 3100.